3D Visualization of Macromolecule Synthesis

Timothy J. Duerr¹, Ester Comellas^{2,3}, Eun Kyung Jeon¹, Johanna E. Farkas¹, Marylou Joetzjer⁴, Julien Garnier⁴, Sandra J. Shefelbine^{3,5}, James R. Monaghan^{1,*}

³Mechanical and Industrial Engineering, Northeastern University, Boston, MA 02115, USA

⁴University of Technology of Compiègne, Rue Roger Couttolenc, 60200 Compiègne, France

¹Department of Biology, Northeastern University, Boston, MA 02115, USA

²Department of Mathematics, Laboratori de Càlcul Numeric (LaCàN), Universitat Politècnica de Catalunya (UPC), 08034 Barcelona, Spain

⁵Department of Bioengineering, Northeastern University, Boston, MA, USA

 $[\]hbox{$*$ Author for correspondence (j.monaghan@northeastern.edu)}\\$

Abstract

1

- 2 Measuring nascent macromolecular synthesis *in vivo* is key to understanding how cells and
- 3 tissues progress through development and respond to external cues. Here, we perform in vivo
- 4 injection of alkyne- or azide-modified analogs of thymidine, uridine, methionine, and
- 5 glucosamine to label nascent synthesis of DNA, RNA, protein, and glycosylation. Three-
- 6 dimensional volumetric imaging of nascent macromolecule synthesis was performed in axolotl
- 7 salamander tissue using whole mount click chemistry-based fluorescent staining followed by
- 8 light sheet fluorescent microscopy. We also developed an image processing pipeline for
- 9 segmentation and classification of morphological regions of interest and individual cells, and we
- apply this pipeline to the regenerating humerus. We demonstrate our approach is sensitive to
- biological perturbations by measuring changes in DNA synthesis after limb denervation. This
- method provides a powerful means to quantitatively interrogate macromolecule synthesis in
- heterogenous tissues at the organ, cellular, and molecular levels of organization.

Introduction

- 15 The measurement of nascent DNA, RNA, and protein synthesis in animals provides critical
- information on the state of cells (dividing, growing, dying) in relation to their surrounding cells.
- 17 Traditionally, radiolabeled or brominated nucleosides or amino acids are introduced to live
- animals, where they are incorporated into macromolecules during DNA synthesis^{1,2},
- trancription^{3,4}, and translation⁵. Performing such approaches have allowed the characterization of
- 20 cells actively undergoing macromolecular synthesis as well as quantification of synthesis rates,
- 21 which facilitates the study of cell behavior during tissue remodeling, proliferation, stress, or
- disease ⁶⁻⁹.
- 23 In the past decade, bio-orthogonal macromolecule precursor analogs including 5-ethynyl-2'-
- deoxyuridine (EdU), 5-ethynyl-uridine (5-EU), and L-azidohomoalanine (AHA) have become
- commercially available. After injection of macromolecule precursor analogs into animals,
- precursors can later be detected in nascent DNA, RNA, and protein macromolecules with
- 27 fluorescently labeled azides or alkynes through highly selective copper catalyzed azide-alkyne
- 28 cycloaddition ("click") chemistry 10-12. These powerful new analogs provide an alternative to the
- use of dangerous isotopes and the challenges associated with brominated precursors such as the

30 requirement of large secondary antibodies (~150kd) and harsh tissue retrieval methods that limit 31 their use in whole tissue samples. 32 Advantages of the click-chemistry labeling approach include the inert nature of macromolecule 33 precursor analogs that have minimal impact on the animal, the small size of fluorescently labeled 34 alkynes and azides, and the high selectivity of click-chemistry. These advantages have enabled whole mount fluorescent labeling of DNA synthesis¹¹, RNA transcription¹³, protein translation¹⁴, 35 36 and glycans^{15,16} in animals. These pioneering proof of principle experiments have demonstrated 37 that imaging macromolecular synthesis is possible, but the fact that most model organisms are 38 large, optically opaque, and consist of heterogenous tissues has made it a challenge to image 39 biological phenomena in deep tissues. Challenges such as photon penetration, differences in 40 refractive indices among different cellular components, light-induced photodamage, and 41 background fluorescence have limited the use of whole mount imaging of macromolecular 42 synthesis. 43 Advances in light sheet fluorescence microscopes (LSFMs) have recently enabled the imaging of large biological specimens from millimeters to several centimeters in size¹⁷. LSFMs have been 44 45 utilized for volumetric imaging of many varieties including visualization of mRNA in whole mount fluorescence in situ hybridization experiments¹⁸ and in vivo interrogation of deep tissue 46 dynamics in transgenic reporter animals¹⁹ among others¹⁷. Clearing methods like CLARITY²⁰, 47 CUBIC²¹, and 3DISCO²² have further enabled volumetric imaging by decreasing refractive index 48 49 mismatches and tissue clearing to advance large specimen imaging even further. Together, the 50 rise of three-dimensional imaging, new staining techniques, and tissue clearing has demanded 51 new means for cell counting, segmentation, and fluorescence quantification. 52 Here, we present a click-chemistry based method to visualize DNA synthesis, transcription, 53 translation, and protein glycosylation in whole mount samples using LSFM (Figure 1A). We 54 demonstrate the utility of this technique by imaging macromolecular synthesis in the 55 regenerating axolotl salamander limb. Following limb amputation, the axolotl regenerates its limb by generating a mass of proliferating cells at the limb stump called a blastema²³. The 56 57 blastema is an ideal environment to test our method because it is an accessible, heterogenous

tissue that increases DNA synthesis, transcriptional output, and translation rates compared to

- 59 uninjured tissue. Furthermore, DNA, RNA, and protein synthesis decrease after denervation of
- the regenerating $limb^{24,25}$.
- We use the regenerating limb to demonstrate that two click-it ready precursors can be
- administered and subsequently visualized simultaneously in a single sample. We also show that
- optical resolution of images can be improved with the clearing agent 2,2'-thiodiethanol (TDE),
- and that this method works in a number of tissues. We outline an image analysis pipeline for
- 65 three dimensional (3D) morphology segmentation, cell counting, and fluorescence quantification
- of stained tissues. We apply this pipeline to the regenerating humerus to demonstrate the
- 67 multiscale quantitative analysis capabilities of our method. Finally, we show that our method is
- sensitive enough to detect and quantify changes in DNA synthesis rates in whole mount
- 69 innervated and denervated regenerating limbs. Taken together, our method provides a unique
- approach to simultaneously interrogate cell state at the organ, cellular and molecular levels of
- 71 organization.

Materials and methods

- 73 Animal procedures
- Axolotls (Ambystoma mexicanum: d/d RRID Catalog #101L) were either bred in captivity at
- Northeastern University or purchased from the Ambystoma Genetic Stock Center at the
- 76 University of Kentucky. Experiments were performed in accordance with Northeastern
- 77 University Institutional Animal Care and Use Committee. Animals were grown to 4-6cm (Mean
- 78 5.3cm, SD 0.36) and 1-1.5g (Mean 1.3g, SD 0.19g) for use in all studies. For all experiments,
- animals were anesthetized by treatment of 0.01% benzocaine until visually immobilized. Limbs
- were amputated either at the distal end of the zeugopod or midway through the stylopod, and
- bones were trimmed below the amputation plane to allow for uniform growth. At the date of
- collection, animals were reanaesthetized and injected with either EdU (8.0ng/g animal), 5-EU
- 83 (270.0µg/g animal), AHA (180.59µg/g animal), or N-azidoacetylglucosamine-tetraacylated
- 84 (GlcNAz) (4.3µg/g animal) alone or simultaneously with the following combinations:
- 85 EdU/AHA, EdU/GlcNAz, 5-EU/AHA, 5-EU/GlcNAz. All monomer analogs were purchased
- 86 from www.clickchemistrytools.com and resuspended in DMSO at the following concentrations:
- 87 EdU- 300mM, 5-EU- 100mM, AHA- 100mM, GlcNAz- 100mM. Stocks were further diluted in
- 88 1X phosphate buffered saline (PBS) for injection. Three hours after injection, limbs were

- collected from the upper stylopod and fixed in 4% paraformaldehyde (PFA) (diluted in 1X PBS)
- at 4°C overnight. If limbs were denervated, the nerve supply was severed at the brachial plexus
- 91 24 hours prior to tissue collection.
- 92 Whole mount click-it protocol
- 93 Following fixation in 4% PFA, samples were washed three times with 1X PBS at room
- 94 temperature (~23°C) for 5 minutes. Samples were dehydrated in an increasing methanol series at
- room temperature starting with 25% methanol (diluted in 1X PBS), 50% methanol, 75%
- methanol, and 100% methanol for 5 minutes at each step. Samples could then be stored in 100%
- 97 methanol indefinitely at -20°C. For staining, samples were rehydrated in a decreasing methanol
- 98 series starting with 75% methanol (diluted in 1X PBS), 50% methanol, 25% methanol, and
- 99 finally placed in 100% 1X PBS for 5 minutes at each step. Samples were then washed 3 times
- with 1X PBST (1X PBS with 1% Triton) for 5 minutes at room temperature. To aid in clearing,
- samples were washed in 0.5% trypsin (diluted in 1X PBST) for 30-90 minutes on a rocker at
- 102 room temperature, or until sample appeared translucent. Samples were washed three times at
- room temperature for 5 minutes with deionized water, then washed in 100% acetone for 20
- minutes at -20°C and washed with deionized water again for 10 minutes. Samples were washed
- in 1X PBST three times at room temperature for 5 minutes prior to applying click-it cocktail for
- 30 minutes at room temperature. The click-it cocktail was made in 1X TRIS buffered saline as
- 107 follows: 50µL 100mM Sodium Ascorbate, 20µL 4mM CuSO₄, and 2µL 500µM azide- or
- alkyne-modified Alexa Flour, combined in order as listed. After the first round of staining,
- samples were washed at room temperature 6 times for 30 minutes with rocking. For double-
- labelling, samples were again placed in the click-it cocktail with a different fluorescent dye to
- stain for the second analog at room temperature overnight. Both rounds of staining were
- 112 conducted in the dark to prevent photodegradation of fluorescent molecules. For staining with
- DAPI, samples were washed 3 times for 5 minutes with 1X PBS, then placed in 277mM DAPI
- for 4 days at room temperature. Samples were washed 3 times for 20 minutes with 1X PBS and
- left in 1X PBS at 4°C for short term storage prior to imaging with LSFM. Whole mount samples
- were cleared with 67% TDE (diluted in deionized water) overnight at room temperature in the
- 117 dark.
- 118 Tissue section click-it protocol

119 Following fixation in 4% PFA, samples were washed three times in 1X PBS each for 5 minutes, 120 and cryoprotected in 30% sucrose on a rocker for 1 hour or until the tissue fully sinks. Samples 121 were removed form sucrose and briefly washed in optimal cutting temperature (OCT) compound 122 before mounting in OCT compound and frozen at -80°C. 10µm sections were obtained using a 123 cryostat and baked at 65°C for 15 minutes. Slides were then washed with water for 30 minutes at 124 room temperature to remove residual OCT. Slides were washed once with 1X PBS for 5 minutes 125 at room temperature. The click-it cocktail (same as above) was applied to the slides and 126 incubated at room temperature in the dark for 30 minutes. If staining for a second 127 macromolecule, slides were washed five times for 5 minutes with 1X PBS at room temperature. 128 The samples were then stained for 30 minutes at room temperature in the dark using the above 129 click-it cocktail with a different a fluorophore dye. Following the final click-it reaction, slides 130 were washed once with 1X PBS at room temperature for 5 minutes, then stained with 277mM 131 DAPI for 5 minutes at room temperature. Slides were washed again with 1X PBS for 5 minutes 132 at room temperature and water for 5 minutes at room temperature and mounted with SlowFadeTM 133 Gold Antifade Mountant (Thermo S36936). Slides were imaged using a Zeiss LSM800 confocal 134 microscope. 135 Light sheet microscopy 136 All 3D images were acquired using a Zeiss light sheet Z.1 microscope paired 137 with Zen software. Unless otherwise indicated, samples were cleared and imaged in 67% TDE. 138 Post-processing for visualization purposes was performed with Arivis Vision4D v3.1.4 on 139 a workstation with a 64-bit Windows Embedded Standard operating system, and an Intel(R) 140 Xeon(R) CPU E5-2620 v3 @ 2.40GhZ (2 processors), 128GB RAM, and NVIDIA Quadro 141 K2200 GPU. Sub-volumes were stitched together with the Tile Sorter in Arivis, using the manual 142 projection option. Volume fusion was performed through automatic landmark registration of 143 manually selected points for alignment. Finally, constant background intensity was corrected 144 using the automatic functionality. 145 Data analysis All data were processed on desktop computers with the aid of Fiji²⁶ and Matlab²⁷. The custom 146 147 Fiji scripts and Matlab codes used are available in the supplementary material. We performed all

analyses on unprocessed .czi files acquired directly from the light sheet microscope.

149 Organ level: The goal of the organ level analysis was to determine gross morphology of the 150 organ, such as area, principal axes, and maximum diameters in said axes for each cross section. 151 Critical to this step is alignment of the images to a standard defined axis and reslicing in the 152 transverse direction (perpendicular to the long axis of the humerus). The image stack of a 153 regenerating axolotl elbow was imported into Fiji and aligned along the proximodistal axis of the 154 humerus (Figure 3A). Morphological segmentation of the humerus was performed semi-155 automatically with the Segmentation Editor plugin (Figure 3B). The segmented surface was then exported from Fiji as a mesh via an .stl file using 3D Viewer²⁸. Volumetric analysis was 156 157 performed in Fiji by reslicing the aligned mask (Figure 3B) to obtain a stack of cross-sections 158 perpendicular to the proximodistal axis, and then quantified the shape and volume with the Slice Geometry option in the BoneJ²⁹ Fiji plugin. Slice Geometry calculates cross-sectional geometric 159 160 properties of shapes, including area, second moment of area around the major and minor axes, 161 and maximum chord length from these major and minor axes. 162 Cellular level: The goal of the cellular level analysis was to determine the number of 163 proliferating cells (EdU⁺) as a function of proximodistal position along the humerus, as well as 164 average size, shape, and orientation. The aligned image stack (Figure 3A) was cropped using the 165 morphological segmentation (Figure 3B) as a mask with the aid of the Image Calculator in Fiji. 166 Based on the EdU staining (Figure 3C), we segmented the nuclei of the proliferating cells with Trainable Weka Segmentation 3D³⁰. We used a combination of filters available in Fiji before and 167 168 after training the algorithm to improve segmentation results. Filters applied include the 3D Edge 169 and Symmetry, Background Subtraction, 3D Fill Holes, Gaussian Blur 3D, and 3D Watershed 170 Split. A detailed description of the sequence and parameters used is available in the 171 supplementary materials. The 3D Objects Counter then provided a list of identified cells as well 172 as their volume and position, among other information. In addition, the surfaces of the 173 segmented cell nuclei were exported and processed in MeshLab, similarly to the process 174 followed with the organ segmentation, to be visualized in Matlab (Figure 3E). The centroid 175 coordinates and corresponding object volumes identified in Fiji were imported into Matlab for 176 further processing and plotting. We computed the number of cell centroids within 50µm thick 177 slices perpendicular to the proximodistal axis to obtain a density-like measure of proliferating 178 cells. Slice thickness was selected as slightly larger than the average cell diameter to ensure cells 179 were not sampled across more than two slices.

Molecular level: The goal of the molecular level analysis was to determine molecular activity, characterized by fluorescent signal, which in our study represented DNA replication (EdU). The aligned and cropped image stack used as a starting point of the cellular-level analysis (Figure 3C) was also analyzed at the molecular level. We resliced the image stack along the proximodistal axis in the organ under study (Figure 3F). The histogram and pixel intensity statistics were listed for each slice via the getRawstatistics function. These allow for further quantification of the fluorescent signal in Matlab, e.g. we calculated the mean intensity of each plane along the proximodistal axis and the histogram of the whole organ. For the example showing nerve-dependent regeneration in axolotl blastemas (Figure 6A), we compared overall pixel intensity of the left (denervated) and right (control, innervated) forelimbs of the same animal. To ensure full repeatability of our data analysis, we selected the same cubic volume in all blastemas processed: a cube with 175µm sides, centered along the proximal-distal axis and at a distance of 250µm from the distal tip (Figure 6A). The cube size was adjusted to maximize the cube volume for all blastemas processed, while ensuring that the entire cube was contained within the blastema. Histograms of each cubic volume and the ratio between the innervated and denervated limb of the same animal were computed and plotted with Matlab (Figure 6B) to quantify the changes in proliferation in innervated versus denervated limbs at different stages of regeneration. All scripts for blastema cube quantification are provided in the supplementary materials.

Results and discussion

180

181

182

183

184

185

186

187

188

189

190

191

192

193

194

195

196

197

198

199

200

201

202

203

204

205

206

207

208

209

Whole mount, click-it based visualization of macromolecule synthesis

To visualize macromolecule synthesis, we injected click-it compatible monomer analogs (Table 1) intraperitonially three hours prior to sample collection. During this time, analogs metabolically incorporated into nascently synthesized macromolecules, resulting in *in vivo* labeling of macromolecule synthesis. These labeled macromolecules contain either azide- or alkyne-modified monomers that can be detected with click-it compatible fluorescent molecules, enabling imaging of nascent macromolecules in whole mount tissues with LSFM (Figure 1). To demonstrate the multiplexing capabilities of the approach, modified monomer analogs with disparate functional groups (EdU/AHA, 5-EU/AHA, EdU/GlcNAz, 5-EU/GlcNAz) were coinjected and visualized with LSFM (Figure 2A-D, Supplementary videos 1-2). Whole mount

210 samples were comparable to 2D longitudinal tissue sections of the same stains (Figure 2I-L), 211 showing that our method generates similar results in both whole mount and tissue sections 212 (Supplementary Figure 1). We demonstrate the specificity of N-Acetylglucosamine (GlcNAc) 213 incorporation by showing that a GlcNAz-specific antibody pretreated on tissue sections collected 214 from GlcNAz injected animals prevented the subsequent click-it reaction (Supplementary Figure 215 2). 216 An advantage of our method is that staining whole mount tissues eliminates the need for 217 sectioning, reducing the potential inconsistences that arise as a result of the sectioning process 218 (uneven tissue, different cutting planes, etc.). Additionally, traditional methods of obtaining 3D 219 images of thick tissues with confocal microscopy are impractically slow when imaging hundreds 220 of images in a single stack. LSFM allows for more rapid imaging of whole samples, requiring 221 only minutes to image each sample. However, several considerations exist when imaging whole 222 tissue in 3D with LSFM. Stain penetrates slower in whole 3D tissues compared to 10-20µm thick 223 tissue sections, requiring longer staining times. An advantage of our method is that the click 224 reaction requires molecularly diminutive reagents that readily pass through cell and nuclear 225 membranes, ensuring stain penetration in the center of dense tissues. Different refractive indices 226 between disparate cellular components and the imaging media cause light to scatter, which can reduce the resolution and brightness of 3D images³¹. To improve image resolution and light 227 228 penetration, overnight refractive index matching with 67% 2,2'-thiodiethanol (TDE) can 229 sufficiently clear axolotl limbs for imaging with LSFM. This clearing method rapidly and 230 effectively improves the signal to noise ratio of stained samples compared to imaging in PBS 231 (Supplementary Figure 3). With careful attention to these challenges, our method provides a 232 means to obtain high quality 3D images from tissues 1mm in depth in less than 10 minutes per 233 sample (Figure 2A-H) with clear, consistent staining. 234 3D, multiscale quantitative analysis of the regenerating humerus 235 To demonstrate that our whole mount click-it method can obtain quantifiable data on the organ, 236 cellular, and molecular levels of organization, we applied our technique to the regenerating 237 humerus. After regenerating for 35 days, axolotls with mid-humeral amputations were injected 238 with EdU/AHA to identify cells within the humerus undergoing DNA synthesis (EdU) and 239 protein translation (AHA). We observed EdU staining in chondrocytes distal to the amputation

240 plane and AHA staining in the humerus perichondrium (Figure 3A). We outline a multiscale, 241 quantitative pipeline that leverages the staining patterns of these macromolecules for analysis of 242 3D humerus morphology and 3D macromolecule synthesis. This workflow combines available plugins in Fiji²⁶ and scripts developed in Fiji and Matlab²⁷ for the data analysis process (see 243 supplementary information for a detailed description). 244 245 For 3D organ level analysis of macromolecule synthesis, AHA staining provided an adequate 246 outline of the humerus, allowing us to segment its 3D morphology (Figure 3A-B). We quantified 247 organ shape by assessing cross-sectional area (Figure 4A') and circularity (Figure 4A'') of the segmented humerus along the proximodistal axis with BoneJ²⁹ (Figure 4A). These measurements 248 249 of 3D organ size can be obtained with other methods such as microCT and focused ion beam 250 scanning electron microscopy (FIB-SEM). However, microCT is unable to image every tissue 251 due to stain limitations and uses hazardous radiation, while FIB-SEM can capture 3D surface 252 topography but not the entire organ morphology. Our method has the capability to fully image 253 the 3D structure of entire organs (size permitting) without the need for radiation while 254 simultaneously capturing information from both the cellular and molecular levels of 255 organization. 256 On the cellular level, we segmented the 3D morphology of proliferating chondrocytes based on EdU staining using the Trainable Weka Segmentation 3D plugin³⁰ (Figure 4B"). With this 257 258 segmentation, we identify highly condensed regions of cells undergoing rapid rates of DNA 259 synthesis (Figure 4B). From these data, we observe cells synthesizing DNA most abundantly 260 distal to the plane of amputation, as expected for dividing chondrocytes. Traditionally, cell 261 quantification as such is conducted on 2D tissue sections. In heterogenous tissues, however, cells 262 are distributed non-uniformly; 2D sampling may not accurately capture the cellular distribution 263 and cannot be used to determine cell volume or shape. Our whole mount staining method allows 264 quantification of cells within an entire 3D tissue, resulting in a more accurate assessment of cell 265 density within heterogenous tissues. 266 To demonstrate quantitative molecular analysis of 3D macromolecule synthesis, we assessed 267 staining intensity of EdU in slices along the proximodistal axis of the regenerating humerus (Fig 268 4C). EdU intensity represents the rate at which a cell undergoes DNA synthesis, which is one of 269 the first steps of cell division and proliferation. Proliferating cells rapidly synthesize DNA,

270 enabling cells to integrate EdU into nascent DNA strands, providing ample opportunities for 271 covalent linkage of fluorescent molecules to the DNA strand. Thus, higher pixel values within 272 EdU⁺ cells are representative of faster DNA synthesis rates. These data show that EdU intensity 273 is strongest in the regions distal to the amputation plane of the humerus (Figure 4C'), providing a 274 quantitative measure to assess macromolecule synthesis on the molecular level. Within a tissue, 275 cells synthesize macromolecules heterogeneously, reflected by different fluorescence values 276 between cells. Thus, quantifying macromolecule synthesis based on presence/absence of signal 277 instead of fluorescence does not account for variability in macromolecule synthesis rates among 278 cells. To compound this issue, quantifying fluorescence in tissue sections only represents the rate 279 of macromolecule synthesis from a fraction of cells in larger, heterogenous tissues. Our method 280 provides a means to capture this molecular heterogeneity in 3D samples, allowing us to observe 281 whole 3D regions in the regenerating humerus that synthesize DNA more rapidly than others, 282 which further demonstrates the utility of our whole mount click staining method. 283 Taken together, these results demonstrate that our method can provide quantifiable data on the 284 organ, cellular, and molecular levels of organization. This highlights the novelty of our method, 285 as we have not found previous examples of multiscale analysis as outlined here. We foresee this 286 multiscale, quantitative analysis having broad applications in the examination of dynamic cell 287 processes in 3D, such as in cancer metabolism and mammalian neurogenesis or other fields 288 where macromolecule synthesis is traditionally studied in tissue sections. 289 3D, molecular analysis of biological perturbations 290 To demonstrate that our method is sensitive enough to detect subtle changes in macromolecule 291 synthesis in vivo, we quantified the difference in EdU intensity between limbs regenerating with 292 and without a nerve supply. Cell proliferation in regenerating limbs is sustained by factors secreted from nerves that innervate the limb^{32,33}. Therefore, we amputated both forelimbs at the 293 294 mid-humerus, and the left limb was denervated at the brachial plexus one day prior to collection. 295 At 6, 9, 12, 15, 18, and 25 days post amputation (dpa) animals were pulsed with EdU for 3 hours 296 before collection to label proliferating blastema cells (Figure 5A). LSFM was used to image 297 samples (Figure 5B), ensuring pixel resolution was consistent between samples. We quantified 298 DNA synthesis in denervated limbs compared to innervated limbs by creating a 175x175x175µm 299 cube 250µm from the distal most tip of the blastema (Figure 6A). From these results, we

observed a marked decrease in blastema EdU incorporation due to denervation at 9, 12, and 15dpa (Figure 6B), demonstrating that our whole mount staining approach is capable of detecting changes in macromolecule synthesis after biological perturbations. One potential limitation of our method in the blastema is the inability to preform single cell segmentation. We predict that imaging with higher magnification may overcome this limitation but will significantly increase imaging time and file size.

Conclusions

300

301

302

303

304

305

306

307

308

309

310

311

312

313

314

315

316

317

318

319

320

321

322

323

324

325

326

327

328

329

The work presented here provides a fast, simple pipeline for visualizing macromolecule turnover in the 3D space of whole tissues. While tissue sections were previously the standard for studying these cellular processes, a new standard in the field must be expected where dynamic processes like macromolecule synthesis are visualized in 3D to obtain a more complete understanding of how these processes occur in a larger tissue context. Few modalities of imaging exist to provide this level of analysis. Here, we outline a method to study macromolecule synthesis at the organ, cellular, and molecular levels of organization, which is important in understanding cell state and how cell state affects neighboring cells and tissues. To this end, we show that DNA synthesis, transcription, translation, and protein glycosylation increase in the entire 3D space of the regenerating blastema after limb amputation and that these processes can be visualized concurrently. We outline a multiscale pipeline for analysis and quantification of heterogeneous tissues at the organ, cellular, and molecular levels of organization. Additionally, we demonstrate that our method is sensitive to detect biological perturbations by showing a decrease in DNA synthesis in the blastema following limb denervation. We foresee our method being used to similarly readdress other classical questions with modern techniques for a more exhaustive understanding of biological processes; traditional questions within the fields of cancer biology and neurobiology may especially benefit from a technology as such. Additionally, as more clickit ready macromolecules monomer analogs are generated, our method will provide a means to study more biological processes in whole tissues.

Acknowledgements

The authors would like to acknowledge Tyler Jensen for his early assistance in developing the whole mount staining protocol, and both Alex Lovely and Gouxin Rong for their microscopy and image analysis assistance. Images obtained from the Harvard University Center for Biological

330	Imaging and the Northeastern University Chemical Imaging of Living Systems core. We
331	acknowledge animal support from the Ambystoma Genetic Stock Center funded by NIH grant
332	P40-OD019794.
333	Author Contributions
334	SJS and JRM conceived and supervised the study. TJD, EKJ, and JEF preformed experiments
335	and imaging. EC, MJ, and JG designed and implemented codes for multiscale data analysis. TJD
336	and EC performed the analysis. TJD, EC, SJS, and JRM wrote the paper. All authors approved
337	the final version of the manuscript.
338	Funding
339	This project has received funding from the National Science Foundation under grant #1727518
339340	This project has received funding from the National Science Foundation under grant #1727518 to SJS, #1656429 and #1558017 to JRM. E.C acknowledges funding from the European Union's
340	to SJS, #1656429 and #1558017 to JRM. E.C acknowledges funding from the European Union's
340 341	to SJS, #1656429 and #1558017 to JRM. E.C acknowledges funding from the European Union's Horizon 2020 research and innovation program under the Marie Skłodowska-Curie grant
340341342	to SJS, #1656429 and #1558017 to JRM. E.C acknowledges funding from the European Union's Horizon 2020 research and innovation program under the Marie Skłodowska-Curie grant agreement No. 841047. EKJ acknowledges support from a Northeastern University Matz

References

- 347 1 Sidman, R. L., Miale, I. L. & Feder, N. Cell proliferation and migration in the primitive ependymal zone: an autoradiographic study of histogenesis in the nervous system. *Exp Neurol* **1**, 322-333, doi:10.1016/0014-4886(59)90024-x (1959).
- Gratzner, H. G. Monoclonal antibody to 5-bromo- and 5-iododeoxyuridine: A new reagent for detection of DNA replication. *Science* **218**, 474-475, doi:10.1126/science.7123245 (1982).
- Uddin, M., Altmann, G. G. & Leblond, C. P. Radioautographic visualization of differences in the pattern of [3H]uridine and [3H]orotic acid incorporation into the RNA of migrating columnar cells in the rat small intestine. *J Cell Biol* **98**, 1619-1629, doi:10.1083/jcb.98.5.1619 (1984).
- Wansink, D. G. *et al.* Fluorescent labeling of nascent RNA reveals transcription by RNA polymerase II in domains scattered throughout the nucleus. *J Cell Biol* **122**, 283-293, doi:10.1083/jcb.122.2.283 (1993).
- Garlick, P. J., McNurlan, M. A. & Preedy, V. R. A rapid and convenient technique for measuring the rate of protein synthesis in tissues by injection of [3H]phenylalanine. *Biochem J* 192, 719-723, doi:10.1042/bj1920719 (1980).
- Yoshizawa, F., Nagasawa, T., Nishizawa, N. & Funabiki, R. Protein synthesis and degradation change rapidly in response to food intake in muscle of food-deprived mice. *J Nutr* **127**, 1156-1159, doi:10.1093/jn/127.6.1156 (1997).
- Rombouts, Y. *et al.* Acute phase inflammation is characterized by rapid changes in plasma/peritoneal fluid N-glycosylation in mice. *Glycoconj J* **33**, 457-470, doi:10.1007/s10719-015-9648-9 (2016).
- Brien, T. & Lis, J. T. Rapid changes in Drosophila transcription after an instantaneous heat shock. *Mol Cell Biol* **13**, 3456, doi:10.1128/MCB.13.6.3456 (1993).
- Rose, R. J., Cran, D. G. & Possingham, J. V. Changes in DNA synthesis during cell growth and chloroplast replication in greening spinach leaf disks. *J Cell Sci* **17**, 27-41 (1975).
- 374 10 Kolb, H. C., Finn, M. G. & Sharpless, K. B. Click Chemistry: Diverse Chemical Function 375 from a Few Good Reactions. *Angew Chem Int Ed Engl* **40**, 2004-2021, doi:10.1002/1521-376 3773(20010601)40:11<2004::aid-anie2004>3.3.co;2-x (2001).
- 377 11 Salic, A. & Mitchison, T. J. A chemical method for fast and sensitive detection of DNA synthesis in vivo. *Proc Natl Acad Sci U S A* **105**, 2415-2420, doi:10.1073/pnas.0712168105 (2008).
- Best, M. D. Click chemistry and bioorthogonal reactions: unprecedented selectivity in the labeling of biological molecules. *Biochemistry* **48**, 6571-6584, doi:10.1021/bi9007726 (2009).
- Hinz, F. I., Dieterich, D. C., Tirrell, D. A. & Schuman, E. M. Non-canonical amino acid labeling in vivo to visualize and affinity purify newly synthesized proteins in larval zebrafish. *ACS Chem Neurosci* **3**, 40-49, doi:10.1021/cn2000876 (2012).
- Sawa, M. *et al.* Glycoproteomic probes for fluorescent imaging of fucosylated glycans in vivo. *Proc Natl Acad Sci U S A* **103**, 12371-12376, doi:10.1073/pnas.0605418103 (2006).

- 391 16 Laughlin, S. T. & Bertozzi, C. R. Imaging the glycome. *Proc Natl Acad Sci U S A* **106**, 392 12-17, doi:10.1073/pnas.0811481106 (2009).
- Power, R. M. & Huisken, J. A guide to light-sheet fluorescence microscopy for multiscale imaging. *Nat Methods* **14**, 360-373, doi:10.1038/nmeth.4224 (2017).
- 395 18 Mano, T. *et al.* Whole-Brain Analysis of Cells and Circuits by Tissue Clearing and Light-396 Sheet Microscopy. *J Neurosci* **38**, 9330-9337, doi:10.1523/jneurosci.1677-18.2018 397 (2018).
- Tomer, R., Khairy, K., Amat, F. & Keller, P. J. Quantitative high-speed imaging of entire developing embryos with simultaneous multiview light-sheet microscopy. *Nature Methods* **9**, 755-763, doi:10.1038/nmeth.2062 (2012).
- Chung, K. *et al.* Structural and molecular interrogation of intact biological systems. *Nature* **497**, 332-337, doi:10.1038/nature12107 (2013).
- Susaki, E. A. *et al.* Whole-brain imaging with single-cell resolution using chemical cocktails and computational analysis. *Cell* **157**, 726-739, doi:10.1016/j.cell.2014.03.042 (2014).
- Erturk, A. *et al.* Three-dimensional imaging of solvent-cleared organs using 3DISCO. *Nat Protoc* **7**, 1983-1995, doi:10.1038/nprot.2012.119 (2012).
- 408 23 Stocum, D. L. Mechanisms of urodele limb regeneration. *Regeneration* **4**, 159-200, doi:10.1002/reg2.92 (2017).
- Singer, M. & Caston, J. D. Neurotrophic dependence of macromolecular synthesis in the early limb regenerate of the newt, Triturus. *Journal of Embryology and Experimental Morphology* **28**, 1 (1972).
- Dresden, M. H. Denervation effects on newt limb regeneration: DNA, RNA, and protein synthesis. *Dev Biol* **19**, 311-320, doi:10.1016/0012-1606(69)90044-x (1969).
- Schindelin, J. *et al.* Fiji: an open-source platform for biological-image analysis. *Nature Methods* **9**, 676-682, doi:10.1038/nmeth.2019 (2012).
- 417 27 MATLAB version 9.7.0.813654 (R2019b). Natick, Massachusetts: The MathWorks Inc.; 418 2019
- Pietzsch, T., Saalfeld, S., Preibisch, S. & Tomancak, P. BigDataViewer: visualization and processing for large image data sets. *Nature Methods* **12**, 481-483, doi:10.1038/nmeth.3392 (2015).
- 422 29 Doube, M. *et al.* BoneJ: Free and extensible bone image analysis in ImageJ. *Bone* **47**, 423 1076-1079, doi:10.1016/j.bone.2010.08.023 (2010).
- 424 30 Arganda-Carreras, I. *et al.* Trainable Weka Segmentation: a machine learning tool for microscopy pixel classification. *Bioinformatics* **33**, 2424-2426, doi:10.1093/bioinformatics/btx180 (2017).
- 427 31 Fadero, T. C. & Maddox, P. S. Live imaging looks deeper. *Elife* **6**, e30515, doi:10.7554/eLife.30515 (2017).
- 429 32 Singer, M. The influence of the nerve in regeneration of the amphibian extremity. *Q Rev* 430 *Biol* **27**, 169-200, doi:10.1086/398873 (1952).
- Farkas, J. E. & Monaghan, J. R. A brief history of the study of nerve dependent regeneration. *Neurogenesis (Austin)* 4, e1302216, doi:10.1080/23262133.2017.1302216
- 433 (2017).

434 Table 1. Monomer analogs used to demonstrate whole mount visualization method

Name	Macromolecule	Biological	Click-it	Reference
	analog	process	modification	
5-ethynyl-2'-deoxyuridine	Thymidine	DNA synthesis	Alkyne	Salic &
(EdU)				Mitchison 2008
5-Ethynyl Uridine (5-EU)	Uracil	Transcription	Alkyne	Jao & Salic 2008
L-Azidohomoalanine (AHA)	Methionine	Translation	Azide	Wang et al. 2017
Azide-modified glucosamine	Glucoseamine	Protein	Azide	Laughlin et al.
(GlcNAz)		glycosylation		2006

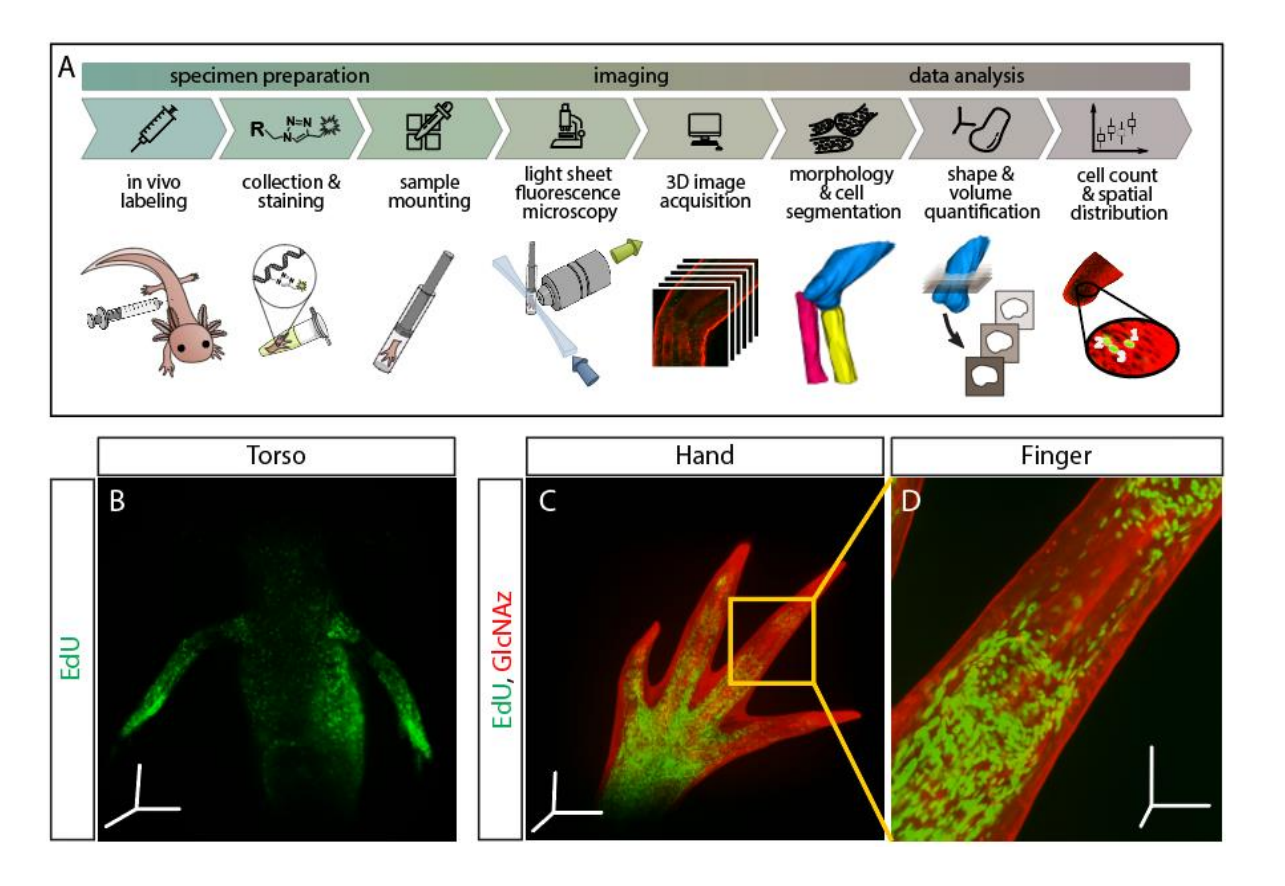


Figure 1. Outline of staining/analysis pipeline and exemplary images.

(A) Overview of entire sample preparation, imaging, and data analysis pipeline. (B-D) Once macromolecules are labeled *in vivo*, synthesis can be visualized throughout the injected animal. Here, we show DNA synthesis (EdU) in the torso (B) and both DNA synthesis and protein glycosylation (GlcNAz) in the hand (C) and finger (D). Images from panels B and C were uncleared and imaged at 5X magnification. Image from panel D was also uncleared and imaged at 10X magnification. Scale bars for panels B&C= 600μm for each axis. Scale bars for panel D= 200μm for each axis.

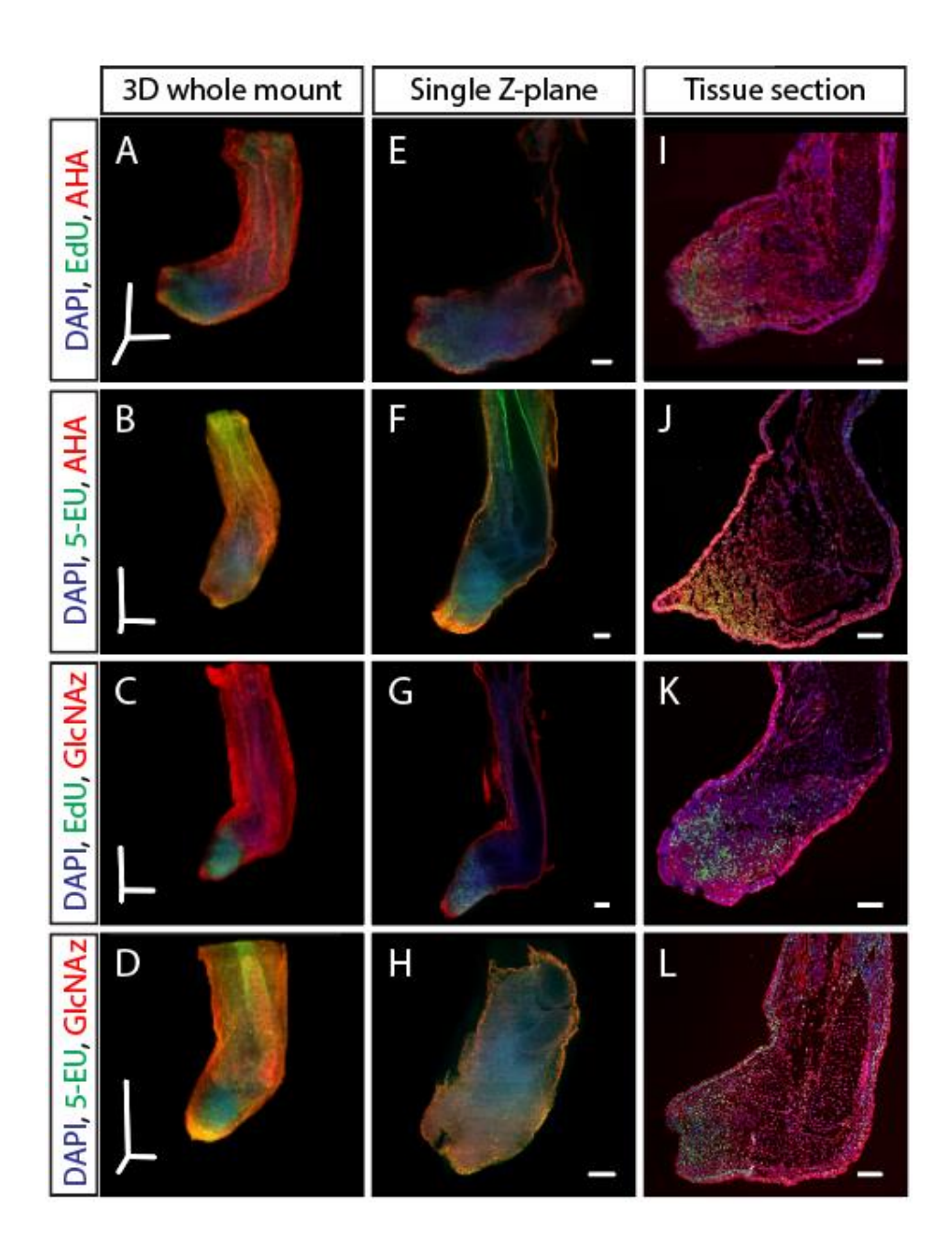


Figure 2. Dual staining of macromolecule synthesis in whole mount.

(A-D) Stitched and fused 3D reconstruction of 13 dpa blastemas stained for multiple macromolecules obtained by LSFM. (B-H) Single Z-plane from A-D that represents the entirety of the blastema. (I-L) Tissue section from identically treated limbs as A-H showing similar macromolecule staining patterns, indicating that the whole mount staining method does not alter macromolecule synthesis staining patterns. Scale bars for panels A-D= 600μ m for each axis. Scale bars for panels E-L= 200μ m.

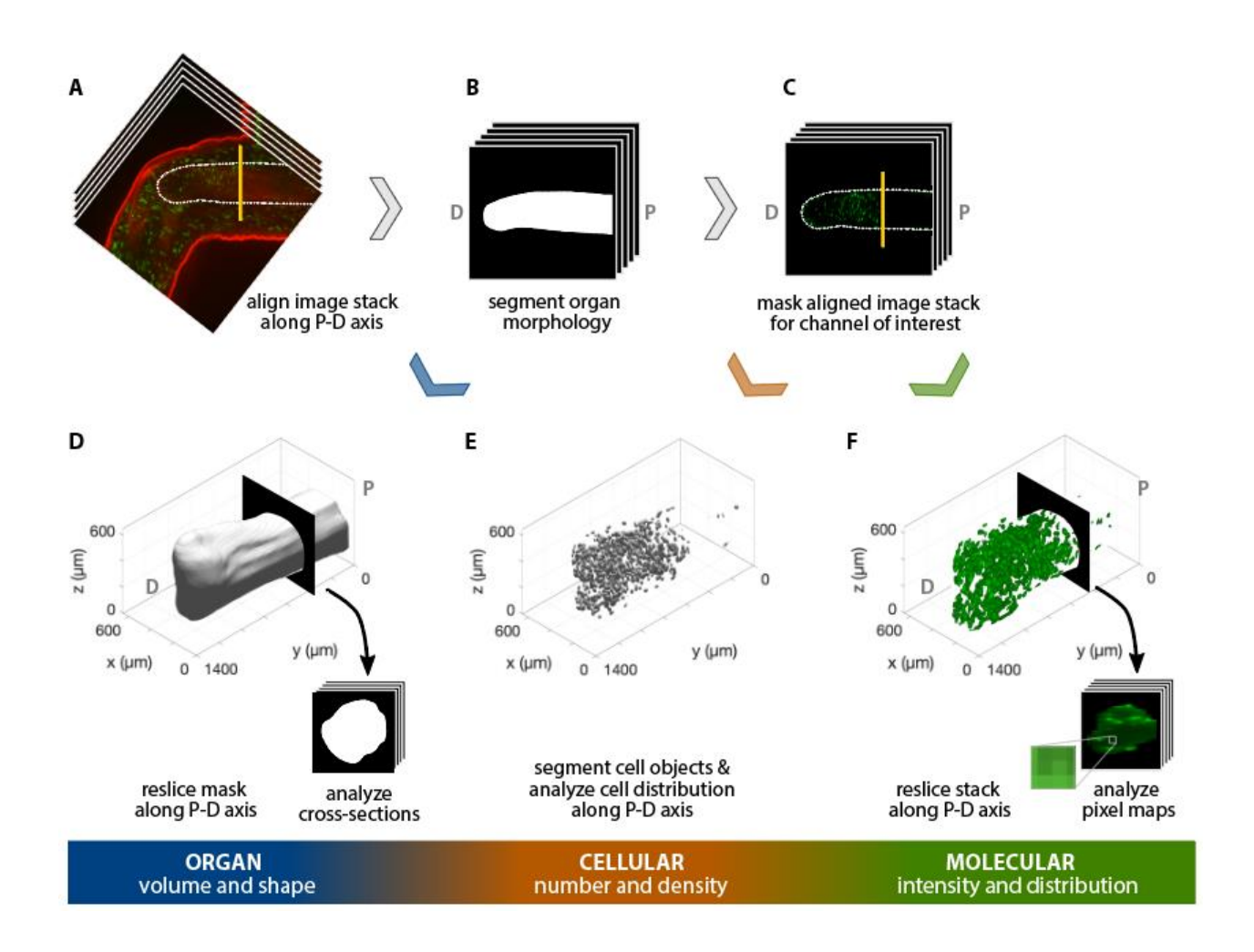


Figure 3. Workflow for 3D, multiscale analysis of the regenerating axolotl humerus.

Multiscale analysis of a 35 dpa regenerating axolotl humerus, stained for AHA (red) and EdU (green). The humerus in the image stack was (A) aligned along the proximodistal (P-D) axis and (B) its morphology was segmented. The resulting mask was used to analyze the organ volume and shape by (D) reslicing it along the P-D axis and studying the cross-sections obtained. (C) The segmented morphology in B was used to mask the green channel for cellular- and molecular-level analyses. (E) Cells in the humerus were segmented and their spatial distribution was analyzed to obtain cellular number and density. (F) The masked image stack in C was resliced along the P-D axis and the pixel maps of the cross-sections were used to characterize the molecular intensity and distribution within the humerus. The vertical yellow line in A and C indicates the plane of amputation.

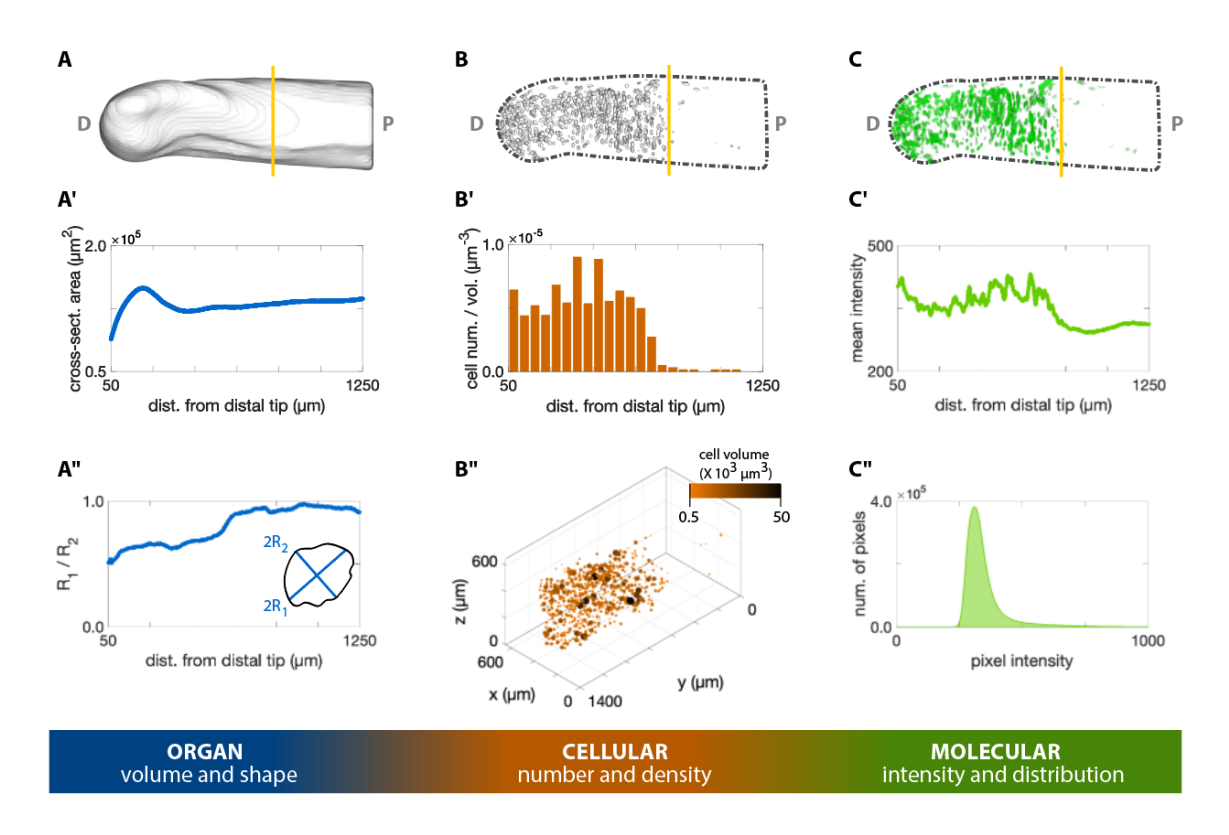


Figure 4. 3D quantification across scales of a regenerating axolotl humerus.

(A) The cross-sections of the humerus in Figure 3D were analyzed with the Fiji plugin BoneJ to quantify humerus shape and volume. (A') The cross-sectional area along the proximodistal (P-D) axis provides a measure of volume distribution along the humerus. (A") The ratio of the maximum chord length from the minor axis $(2R_1)$ with respect to the maximum chord length from the major axis $(2R_2)$ provides a measure of cross-sectional circularity in the humerus. Values closer to 1.0 in the proximal side indicate a more circular cross-section in this zone. (B) The Fiji plugin Trainable Weka Segmentation 3D and 3D Objects Counter were used in the cellular analysis of proliferating chondrocytes illustrated in Figure 3E. (B') The number of EdU+ cells within a 50 μ m slice along the P-D axis was divided by the slice volume to obtain a density-like measure. (B") The center of mass of each cell was plotted in 3D, with point size and color proportional to the segmented cell volume. (C) The molecular intensity and distribution were analyzed based on the resliced pixel intensity maps of the masked green channel in Figure 3F. (C') Mean intensity of each slice perpendicular to the P-D axis. (C") The histogram of the EdU staining in the humerus can provide a measure of DNA synthesis rate. The vertical yellow line in the top row images indicates the plane of amputation.

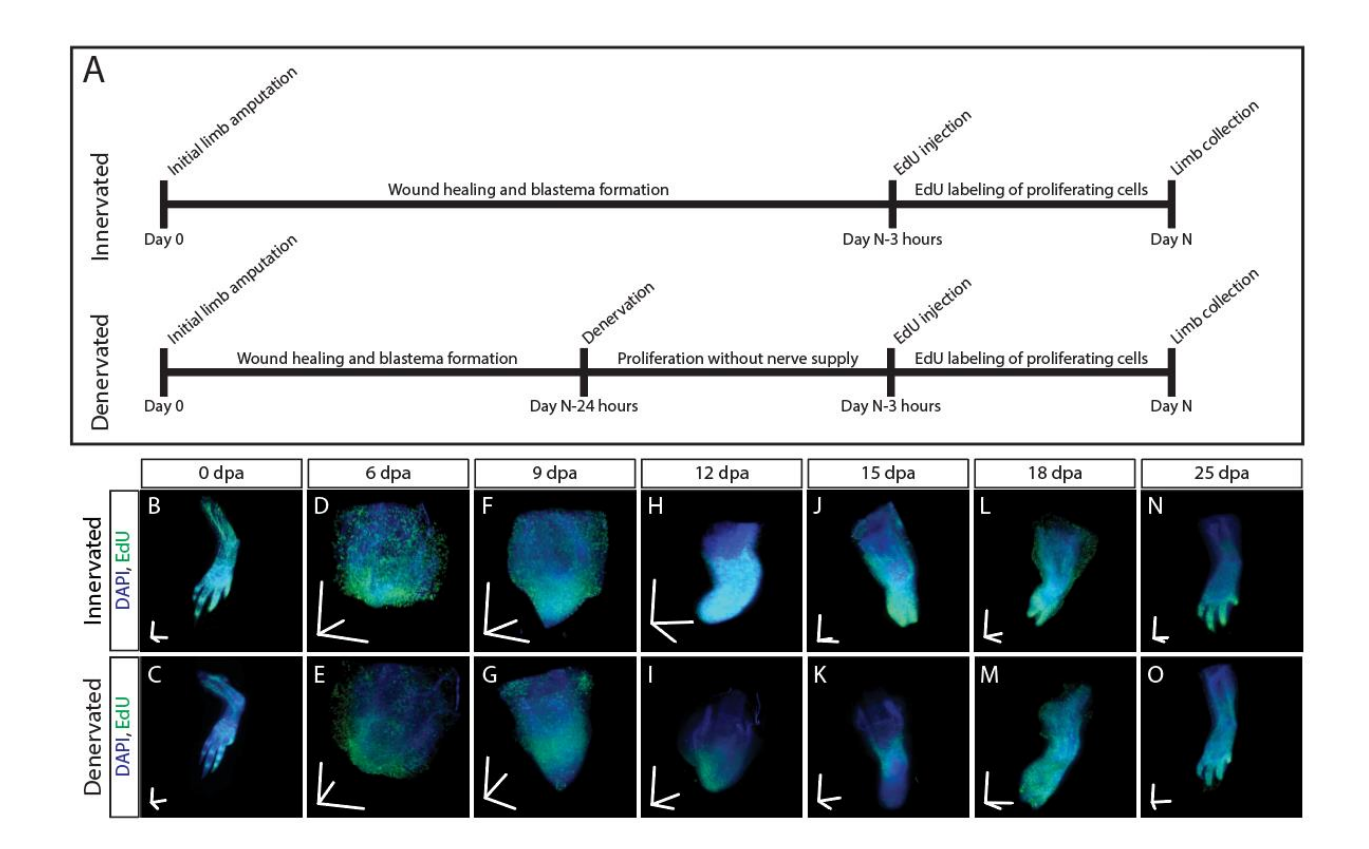


Figure 5. 3D visualization of DNA synthesis in innervated/denervated regenerating limbs.

(A) Schematic of experimental design used to obtain samples from B-O. (B-O) Time course of regeneration in innervated and 24 hour denervated limbs at 0, 6, 9, 12, 15, 18, and 25 dpa. Scale bars for panels B-O= $600\mu m$ for each axis.

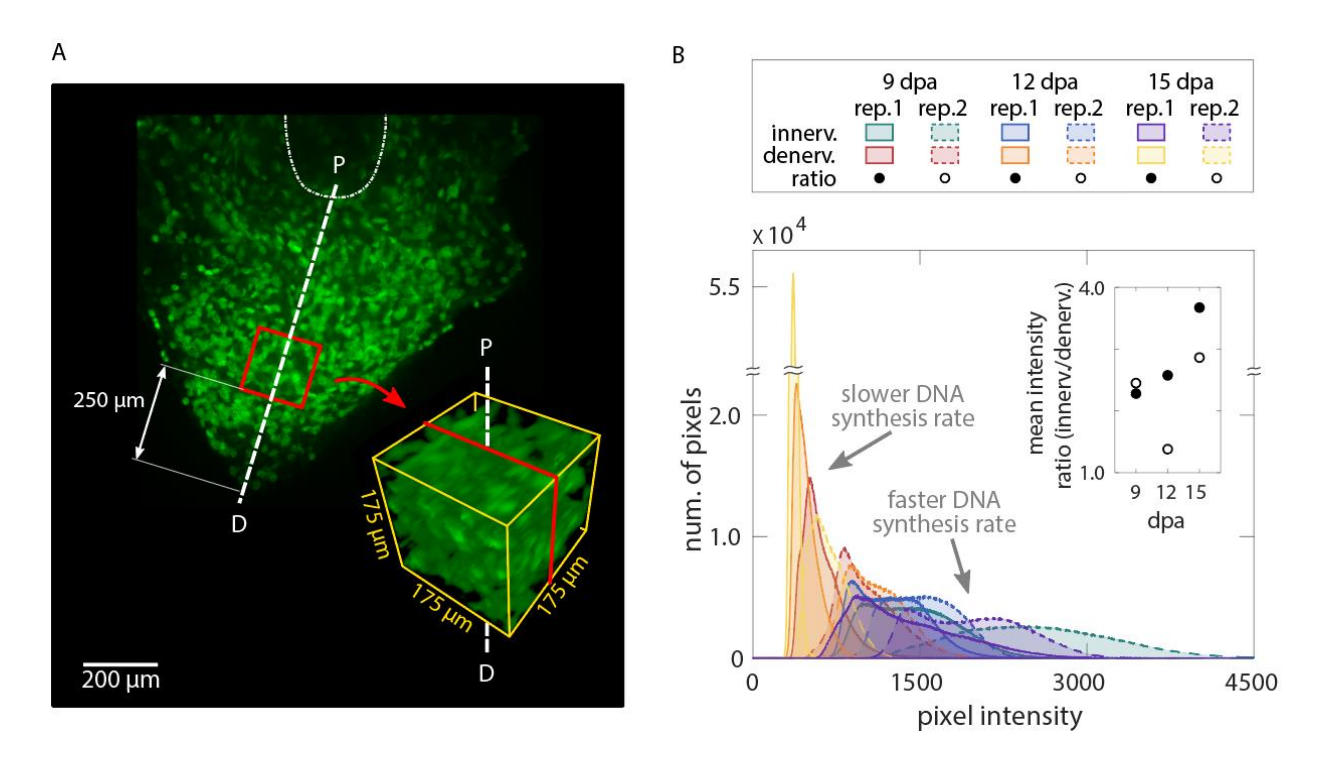
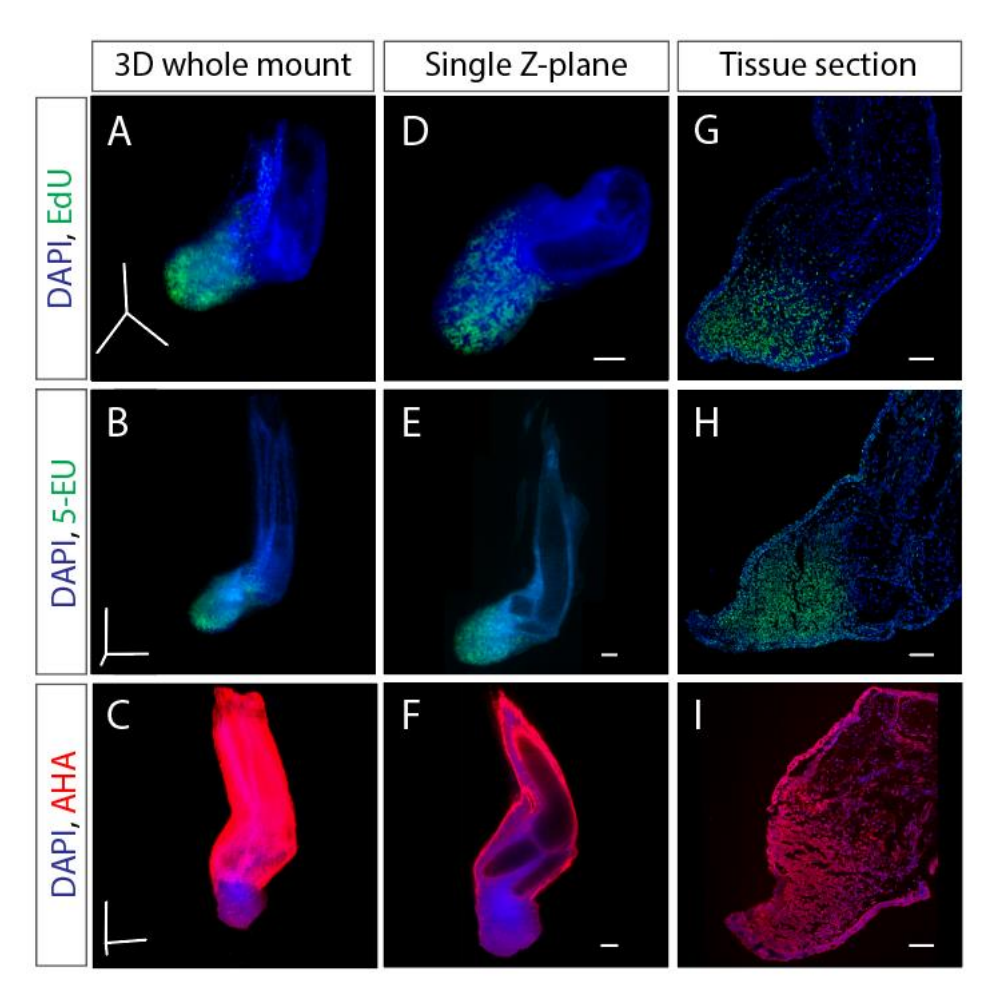


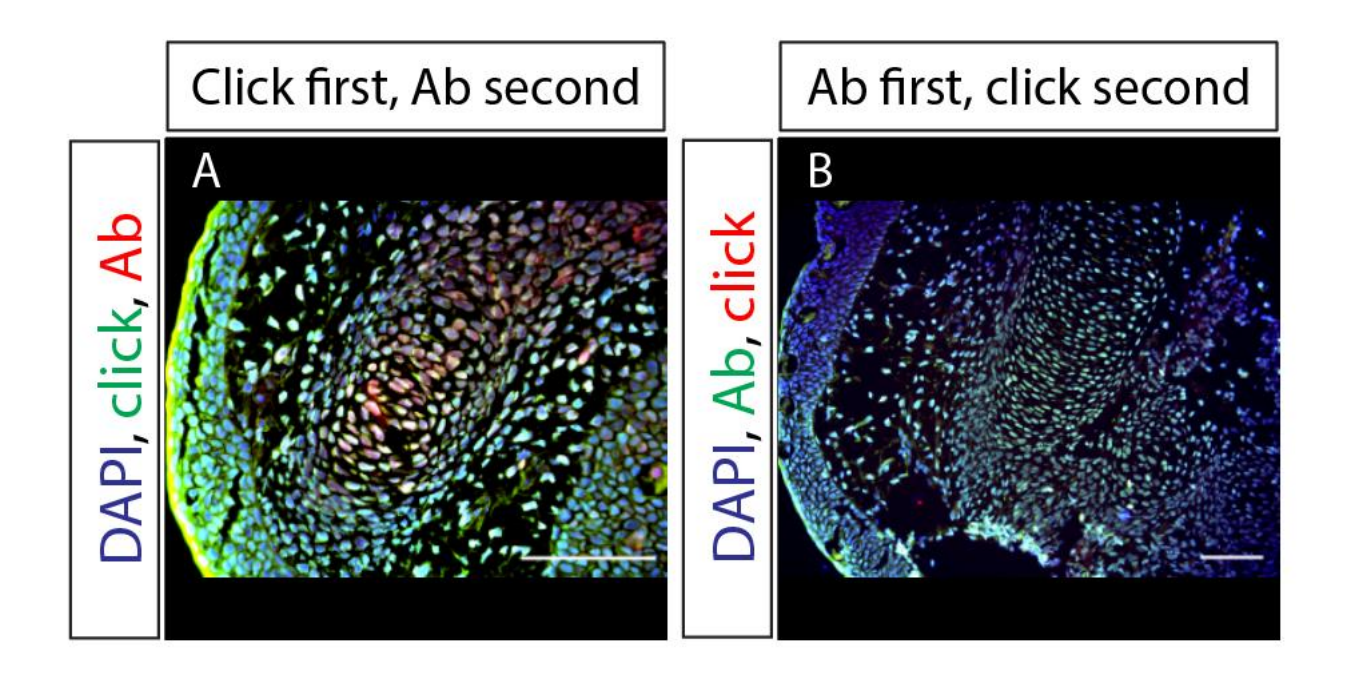
Figure 6. 3D quantification of DNA synthesis in innervated/denervated regenerating limbs.

(A) A cube with sides of 175µm was cropped along the proximodistal axis 250µm from the distal tip of each blastema. (B) The overall histogram of the cubes confirms that innervated blastemas have faster DNA synthesis rates than their denervated counterparts. The difference is quantified by computing the ratio between the mean pixel intensity of the innervated versus denervated blastema cube of a same animal (inset plot).



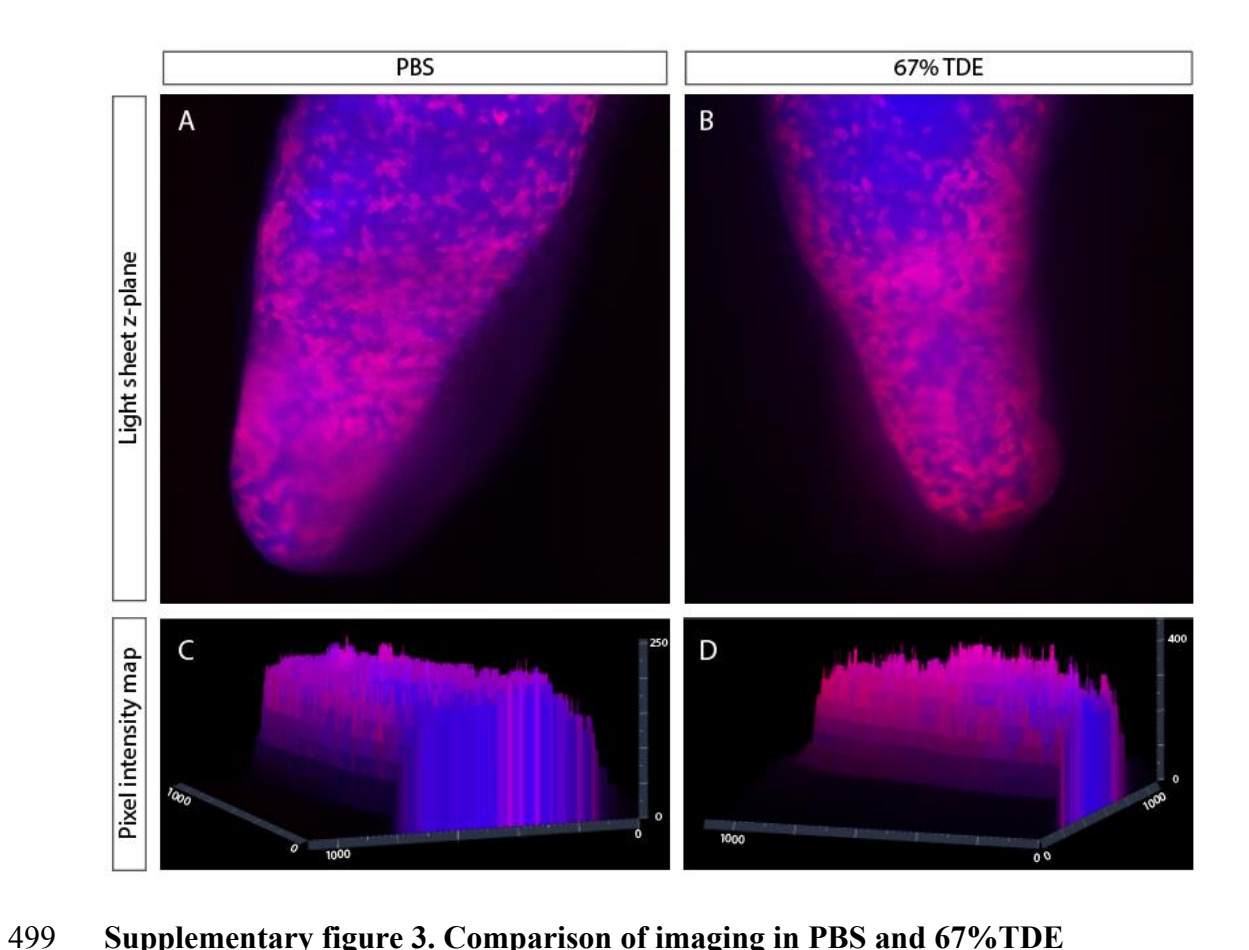
Supplementary figure 1. Single staining of macromolecule synthesis in whole mount.

(A-C) Stitched and fused 3D reconstruction of 13 dpa blastemas stained for one macromolecule obtained by LSFM. (D-F) Single Z-plane from A-C that represents the entirety of the blastema. (G-I) Tissue section from identically treated limbs as A-F. Scale bars for panels A-C= $600\mu m$ in each axis. Scale bars for panels D-I= $200\mu m$.



Supplementary figure 2. Specificity of GlcNAz staining.

(A) Tissue section of a regenerating axolotl limb where the click-it cocktail (green) for GlcNAz was applied prior to staining with GlcNAc antibodies (Ab) (red). (B) Tissue section of a regenerating axolotl limb where GlcNAc antibodies (green) were applied prior to treatment with the click-it cocktail (red) for GlcNAz, demonstrating the specificity of the *in vivo* GlcNAz labeling. Scale bars=100µm.



Supplementary figure 3. Comparison of imaging in PBS and 67%TDE

501

502

503

(A-B) Single Z-plane of 13 dpa blastema imaged in PBS (A) or cleared and imaged in 67% TDE (B). Red indicates EdU staining whereas blue represents DAPI staining. (C-D) Pixel intensity map of PBS imaged blastema (C) and 67% TDE imaged blastema (D). Scale bars are in units of microns.

504	Supplementary video 1
505	Rotating axolotl hand stained for EdU (green) and GlcNAz (red).
506	Supplementary video 2
507	Rotating axolotl limb stained for EdU (green), AHA (red), and DAPI (blue)
508	Supplementary video 3
509	Scroll through of Z-stack from supplementary video 2.